

Accepted Article

Title: A μ -Phosphido Diiron Dumbbell in Multiple Oxidation States

Authors: Franc Meyer, Munmun Ghosh, Hanna H. Cramer, Sebastian Dechert, Serhiy Demeshko, Michael John, Max M. Hansmann, and Shengfa Ye

This manuscript has been accepted after peer review and appears as an Accepted Article online prior to editing, proofing, and formal publication of the final Version of Record (VoR). This work is currently citable by using the Digital Object Identifier (DOI) given below. The VoR will be published online in Early View as soon as possible and may be different to this Accepted Article as a result of editing. Readers should obtain the VoR from the journal website shown below when it is published to ensure accuracy of information. The authors are responsible for the content of this Accepted Article.

To be cited as: *Angew. Chem. Int. Ed.* 10.1002/anie.201908213
Angew. Chem. 10.1002/ange.201908213

Link to VoR: <http://dx.doi.org/10.1002/anie.201908213>
<http://dx.doi.org/10.1002/ange.201908213>

COMMUNICATION

A μ -Phosphido Diiron Dumbbell in Multiple Oxidation StatesMunmun Ghosh,^[a] Hanna H. Cramer,^[b] Sebastian Dechert,^[a] Serhiy Demeshko,^[a] Michael John,^[a] Max M. Hansmann,^[c] Shengfa Ye,^{[d]*} and Franc Meyer^{[a]*}Dedicated to Prof. Goutam K. Lahiri on the occasion of his 60th birthday.

Abstract: Reaction of the ferrous complex $[\text{LFe}(\text{NCMe})_2](\text{OTf})_2$ (**1**) containing a macrocyclic tetracarbene as ligand with $\text{Na}(\text{OCP})$ generates OCP^- ligated complex $[\text{LFe}(\text{PCO})(\text{CO})\text{OTf}]$ (**2**) together with dinuclear μ -phosphido complex $[(\text{LFe})_2\text{P}](\text{OTf})_3$ (**3**) featuring an unprecedented linear $\text{Fe}-(\mu\text{-P})\text{-Fe}$ motif and a "naked" P-atom bridge that appears at +1480 ppm in the ^{31}P NMR spectrum. **3** is shown to exhibit rich redox chemistry, and both singly and doubly oxidized species **4** and **5** could be isolated and fully characterized. X-ray crystallography, UV-vis, EPR and ^{57}Fe Mößbauer spectroscopies in combination with DFT computations provide a comprehensive electronic structure description and evidence that the $\text{Fe}-(\mu\text{-P})\text{-Fe}$ core is highly covalent and structurally invariant over the series of oxidation states that are formally described as ranging from $\text{Fe}^{\text{II}}/\text{Fe}^{\text{III}}$ to $\text{Fe}^{\text{IV}}/\text{Fe}^{\text{IV}}$. **3** – **5** now add a higher homologue set of complexes to many systems with $\text{Fe}-(\mu\text{-O})\text{-Fe}$ and $\text{Fe}-(\mu\text{-N})\text{-Fe}$ core structures that are prominent in bioinorganic chemistry and catalysis.

Stimulated by the great interest in reactive metal-oxido and -nitrido intermediates, substantial efforts have been devoted to isolating transition metal phosphide congeners with a single-atom P_1 unit. Following initial breakthrough reports on molecular compounds with a formal $\text{M}\equiv\text{P}$ triple bond,^[1] a few complexes featuring a terminal or bridging "naked" phosphido ligand have meanwhile been isolated, but almost exclusively for early and mid-transition metals such as Mo and W.^[2] More recently, μ -phosphido linkages have also been structurally authenticated in actinide chemistry.^[3] In contrast, hardly any P_1 -ligated complex has so far been isolated for the most abundant transition metal Fe, even though related oxido-^[4] and nitrido-iron^[5] species are particularly prominent owing to their relevance in bioinorganic chemistry and catalysis.

More generally, molecular complexes with Fe_xP_y cores have remained rare so far. Relevant examples comprise the dinuclear complex **A** with bent $\mu\text{-P}$ linkages and rhombic Fe_2P_2 four-membered ring^[6] as well as a number of systems with larger P_y units derived from white phosphorous (P_4) that feature, e.g., $[\text{Fe}_2(\mu\text{-}\eta^2\text{:}\eta^2\text{-P}_2)_2]$, $[\text{Fe}_2(\mu\text{-}\eta^4\text{:}\eta^4\text{-P}_4)]$ or $[\text{Fe}_4(\mu_4\text{-}\eta^2\text{:}\eta^2\text{:}\eta^2\text{-P}_6)]$ cores.^[7] Driess and Grützmacher *et al* recently reported the synthesis of a mixed-valent ($\text{Fe}^{\text{II}}/\text{Fe}^{\text{III}}$) diiron complex with an asymmetric cyclo- P_3 ligand (**B**) that forms as a product from the reaction of the corresponding chloride- β -diketiminato iron(II) complex and $\text{Na}(\text{OCP})$.^[8] The phosphoethynolate anion (OCP^-)^[9] is emerging as a suitable synthon for transferring P anions. Since practical syntheses of $\text{Na}(\text{OCP})$ and related phosphoethynolate salts have been developed,^[10] this strategy is now being successfully exploited for the preparation of various p-, d-, and f-block metal complexes.^[11]

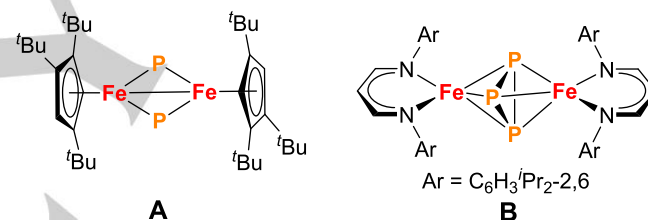


Figure 1. Selected $\text{Fe-P}_y\text{-Fe}$ complexes reported in the literature.^[6,8]

Here we report the reaction of $\text{Na}(\text{OCP})$ with tetracarbene based iron(II) complex $[\text{LFe}(\text{NCMe})_2](\text{OTf})_2$ (**1**; Scheme 1)^[12] and the characterization of the first examples of Fe-P-Fe complexes featuring a single atom "naked" phosphorous bridge between two iron atoms. This now complements the well-known μ -oxido (Fe-O-Fe) and μ -nitrido (Fe-N-Fe) diiron motifs, which hold prominent places in bioinorganic coordination chemistry and beyond.^[4,5] Macrocyclic tetracarbene ligands such as L have previously been shown to serve as a rugged scaffold even under harsh reaction conditions and to support iron complexes in a variety of oxidation states,^[12-16] for example the only organometallic oxoiron(IV) complex $[\text{LFe}(\text{O})(\text{NCMe})](\text{OTf})_2$.^[12,15]

Addition of $\text{Na}(\text{OCP})(\text{dioxane})_{2.5}$ to a suspension of **1** in THF at -35°C resulted in the immediate formation of a green precipitate that turned out to be the μ -phosphido diiron complex $[(\text{LFe})_2\text{P}](\text{OTf})_3$ (**3**; Scheme 1). From the remaining yellow THF solution single crystals of the ferrous complex $[\text{LFe}(\text{PCO})(\text{CO})\text{OTf}]$ (**2**) featuring *trans* positioned OCP^- and CO ligands could be obtained; the molecular structure of the cation of **2** determined by X-ray diffraction is shown in Figure 2 (Figure S48). Metal complexes with intact P-bound OCP^- are quite rare, especially for 3d transition metal complexes.^[17,18]

[a] Dr. M. Ghosh, Dr. S. Dechert, Dr. S. Demeshko, Dr. Michael John, Prof. Dr. F. Meyer
Institut für Anorganische Chemie
Georg-August-Universität Göttingen
Tammannstrasse 4, D-37077 Göttingen (Germany)
E-mail: franc.meyer@chemie.uni-goettingen.de
Homepage: <http://www.meyer.chemie.uni-goettingen.de>

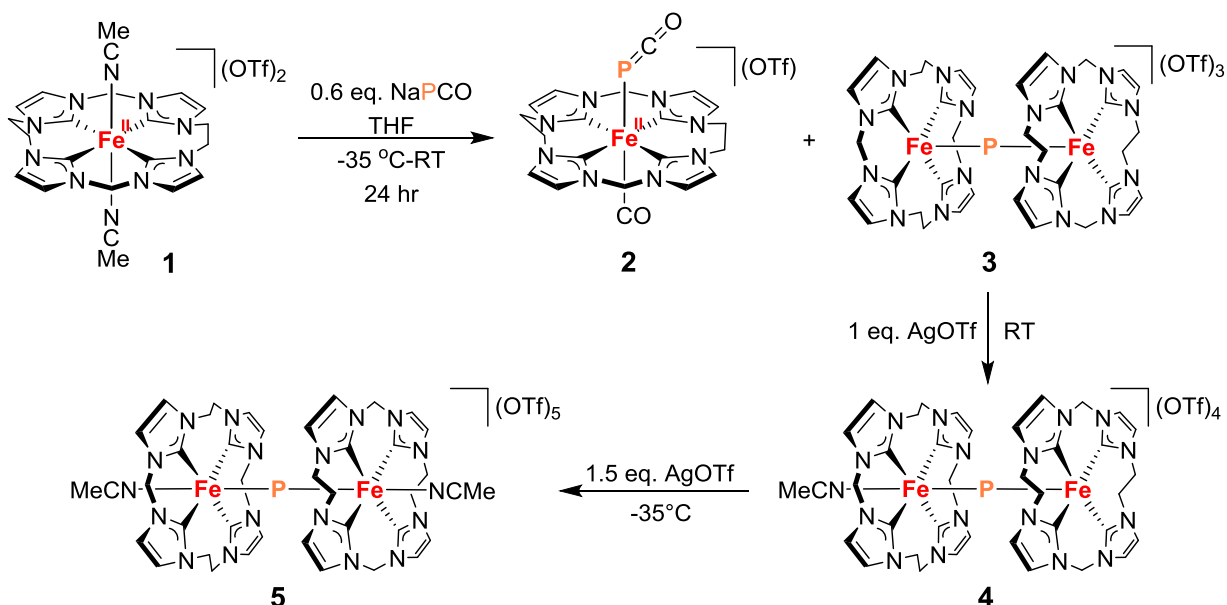
[b] H. H. Cramer
Max-Planck Institut für Chemische Energiekonversion
Stiftstraße 34-36, D-45470 Mülheim an der Ruhr (Germany)

[c] Dr. M. M. Hansmann
Institut für Organische und Biomolekulare Chemie
Georg-August-Universität Göttingen
Tammannstrasse 2, D-37077 Göttingen (Germany)

[d] Dr. S. Ye
Max-Planck Institut für Kohlenforschung
Stiftstraße 34-36, D-45470 Mülheim an der Ruhr (Germany)
E-mail: shengfa.ye@kofo.mpg.de
Homepage: <http://www.kofo.mpg.de/ye>

Supporting information for this article is given via a link at the end of the document.

COMMUNICATION



Scheme 1. Overview of the reactions studied and compounds characterized in this work.

The P–C–O and P–Fe–C angles in **2** are close to 180° (178° & 175°) while the Fe–P–C angle is 95°; Fe–P and Fe–C(O) bond lengths are around 2.50 and 1.74 Å. Note that the Fe–P bond is much longer (~0.5 Å) in comparison to **3** and **5**. As expected, the Fe–C(O) distance is much shorter than the Fe–C^{NHC} bonds of all structurally characterized complexes of this work (1.74 vs. 1.95 to 2.05 Å).

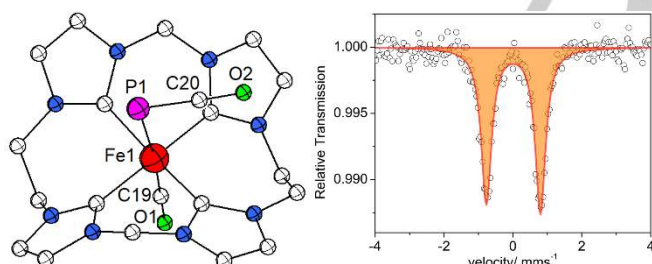


Figure 2. Molecular structure of the cationic part (left) and zero-field ^{57}Fe Mößbauer spectrum of **2** recorded at 80 K (right).

The diamagnetic character of **2** suggests a low-spin d^6 configuration, in line with other six-coordinate ferrous complexes of the tetracarbene macrocycle **L**.^[12,14] The ^{57}Fe Mößbauer spectrum of **2** shows a quadrupole doublet with isomer shift (IS) $\delta = 0.05 \text{ mm s}^{-1}$ and quadruple splitting (QS) $\Delta E_Q = 1.57 \text{ mm s}^{-1}$ (Figure 2, right) and confirms the $S = 0$ spin state. The observed IS is remarkably lower than that of starting low-spin iron(II) complex **1** ($\delta = 0.23 \text{ mm s}^{-1}$, $\Delta E_Q = 2.10 \text{ mm s}^{-1}$),^[12] which reflects the effect of the different π -backbonding abilities of the axial ligands.

Complex **2** in CD_3CN solution at 238 K (also at 298 K) shows a ^{31}P NMR signal at -412 ppm (Figure S1), slightly upfield shifted from the signal of $\text{Na}(\text{OCP})$ in that solvent (-391 ppm). The IR spectrum of **2** (Figure S37) shows a band at 1905 cm^{-1} assigned

to the CO stretch and a band at 1832 cm^{-1} that is assigned to the asymmetric PCO stretching vibration; the latter would suggest a more cumulenic nature of the PCO unit compared to $\text{Na}(\text{OCP})$ (1755 cm^{-1}).^[10a] A ^1H NMR spectrum reflects the apparent C_{2v} symmetry of **2** and reveals pronounced coupling between the P-atom and those H nuclei of the macrocycle methylene groups that are directed towards the OCP^- ligand ($J_{\text{PH}} = 12.47, 7.91 \text{ Hz}$, see Figures S2-S8). In the ^{13}C NMR spectrum, doublets due to coupling to ^{31}P are observed for the adjacent C atom of the OCP^- ligand (at 168.88 ppm, $J_{\text{PC}} = 94.4 \text{ Hz}$), and also for the carbene-C (at 186.33 ppm, $J_{\text{PC}} = 4.5 \text{ Hz}$) and the *trans*-CO ligand (at 222.22 ppm, $J_{\text{PC}} = 9.0 \text{ Hz}$).

Optimizing the synthetic conditions according to the reaction stoichiometry shown in Scheme 1, *viz.* using ~0.6 equivalents of $\text{Na}(\text{OCP})(\text{dioxane})_{2.5}$ and conducting the reaction at -35°C , delivers the two products **2** and **3** in ~60% yield (see SI for details). Diffusion of diethyl ether into a MeCN solution of **3** afforded single crystals suitable for X-ray diffraction. The molecular structure of the cation (Figure 3, top left) shows two {LFe} entities bridged by a single "naked" P atom. The two five-coordinate metal ions are found in a square pyramidal $\{\text{C}_4\text{P}\}$ environment and the central Fe–(μ -P)–Fe core is almost linear (angle Fe–P–Fe 178.3°) with Fe–P bond lengths of 1.993(2) and 1.998(2) Å (Figure S58). These overall structural features are reminiscent of the related oxido-bridged $[(\text{LFe})_2(\mu\text{-O})](\text{OTf})_4$.^[12] The Mößbauer spectrum of **3** shows a quadrupole doublet with parameters $\delta = 0.01 \text{ mm s}^{-1}$ and $\Delta E_Q = 1.94 \text{ mm s}^{-1}$, quite similar to those of $[(\text{LFe})_2(\mu\text{-O})](\text{OTf})_4$ ($\delta = 0.04 \text{ mm s}^{-1}$ and $\Delta E_Q = 2.56 \text{ mm s}^{-1}$)^[12] and indicative of ferric complexes of the tetracarbene macrocycle **L**.^[14] While μ -oxido diiron(III)^[4] complexes are abundant and a number of μ -phosphido complexes have been reported mainly for 4d and 5d metals,^[1a,3a,3c,19] the Fe–(μ -P)–Fe core with a "naked" bridging phosphido ligand is unprecedented.

COMMUNICATION

The ESI(+) mass spectrum of a solution of **3** in MeCN shows a dominant signal for the fragment $[\text{LFe}]^{2+}$ at $m/z = 202.0$ as well as signals at $m/z = 279.5$ and 434.9 assigned to ions $[\text{LFePFeL}]^{3+}$ and $[\text{LFeP}]^+$, respectively. This finding suggests that **3** might disproportionate into ferrous $[\text{LFe}]^{2+}$ and the formal ferryl species $[\text{LFeP}]^+$, at least under ESI-MS conditions (Figure S47). The potential existence of a terminal iron phosphido species $[\text{LFeP}]^+$ is an exciting perspective. It should be noted that a disproportionation equilibrium in MeCN solution has recently been evidenced for diferric $[\text{LFe}^{\text{III}}(\mu\text{-O})\text{Fe}^{\text{III}}\text{L}]^{4+}$, giving **1** and $[(\text{MeCN})\text{LFe}^{\text{IV}}=\text{O}]^{2+}$ (though the equilibrium lies far on the side of $[\text{LFe}^{\text{III}}(\mu\text{-O})\text{Fe}^{\text{III}}\text{L}]^{4+}$; $K_{\text{eq}} = 9.7 \cdot 10^{-7} \text{ M}$).^[13e]

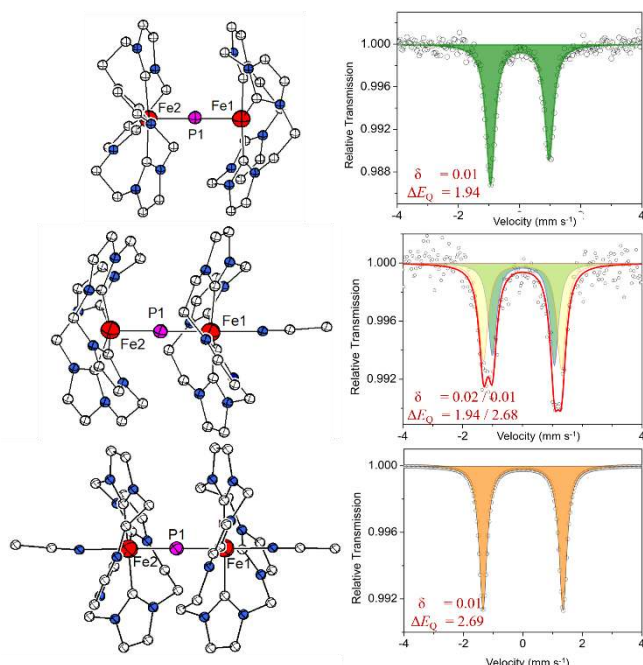


Figure 3. Molecular structures of the cations of **3** (top), **4** (middle) and **5** (bottom) and ^{57}Fe Mössbauer spectra recorded at 80 K of the three compounds (right). IS and QS values (in mm s^{-1}) are given in the respective figure.

Complex **3** is diamagnetic even at room temperature (for SQUID data in the range from 2 to 295 K see Figure S48), indicative of an $S = 0$ ground state and extremely strong antiferromagnetic coupling of the two ferric ions ($|2J| \geq 1200 \text{ cm}^{-1}$), at least as strong as in $[(\text{LFe})_2(\mu\text{-O})](\text{OTf})_4$.^[12] Accordingly, ^1H NMR spectra of **3** in MeCN-d_3 show resonances in the range 3.8 – 7.4 ppm. However, some signals are broad at room temperature but sharpen upon cooling to 238 K, suggesting conformational dynamics of the macrocyclic ligand scaffolds. DOSY in combination with 2D NMR experiments (NOESY, COSY, EXSY, HSQC, HMBC; see Figures S11–S25) at 238 – 298 K identifies three isomers of the trication $[(\text{LFe})_2\text{P}]^{3+}$ that differ by the mutual rotation of the two $\{\text{LFe}\}$ caps and by the conformations of the seven-membered chelate rings, and that interconvert with rate constants between 0.1 and 0.5 s^{-1} at 298 K (derived from ^1H EXSY spectra, Figures S16–S18; see SI for a more detailed discussion). This is reminiscent of the isomerism observed for a derivative of $[(\text{LFe})_2(\mu\text{-O})]^{4+}$ having octamethylated tetracarbene ligands.^[14] In solid state, the two macrocycles L in **3** are rotated by 5° with respect to each other and adopt saddle-shaped conformations

where the $-\text{CH}_2-$ linkages are oriented towards the other $\{\text{LFe}\}$ cap while the $-\text{CH}_2\text{CH}_2-$ linkages are directed outwards, giving approximate (non-crystallographic) D_{2d} symmetry of the complex. Dissolving fresh crystalline material of **3** at 238 K and immediate recording of an NMR spectrum already shows the existence of the three isomers in the solution (two isomers with D_{2d} symmetry, one isomer with C_{2v} symmetry; see SI for details). A DOSY experiment confirmed identical diffusion coefficients for all isomers, $3.016 \times 10^{-10} \text{ m}^2\text{s}^{-1}$, Figure S21). Additional ^1H NMR signals that show exchange with the peaks of the main D_{2d} isomer are observed at 238 K and are found to originate from a (much faster) second dynamic process, namely torsional motion of the ethylene bridges that slows down to about 1 s^{-1} at 238 K.

The ^{31}P NMR spectrum of **3** in MeCN-d_3 at 238 K shows a slightly broadened major signal at +1477.9 ppm and two minor signals at +1492 and +1470 ppm (Figure S10), again reflecting the presence of conformational isomers; a similar peak pattern could also be seen in DMF-d_7 (Figure S14). With increasing temperature the peak at lowest field broadens in both solvents and reaches coalescence with the main peak. A ^{31}P EXSY spectrum (Figure S19) shows exchange between the two peaks (about 300 s^{-1} at 273 K), with population and exchange rates matching those of the isomers with different ethylene bridge torsion detected in the ^1H NMR spectra at 238 K. With a remarkable chemical shift of around +1480 ppm the P nucleus in **3** is even more deshielded than in the $\{\text{Fe}_2\text{P}_2\}$ complex **A** (1407 ppm).^[6b]

Monitoring of the reaction of **1** and $\text{Na}(\text{OCP})$ in DMF-d_7 (where **1** and both products **2** and **3** are soluble) by ^{31}P NMR spectroscopy at room temperature showed only the signals for **2** and **3** (in the expected 1:1 product ratio) already in the first spectrum few minutes after mixing at 238 K (Figure S26). This suggests that the reaction is too fast to detect any intermediates by this method. One may speculate that an initial product $[\text{LFe}(\text{PCO})(\text{NCMe})]^+$ is formed that rapidly releases CO, and the resulting $[\text{LFeP}(\text{NCMe})]^+$ then reacts with starting complex **1** to give **3** (CO release from putative $[\text{LFe}(\text{PCO})(\text{NCMe})]^+$ may also be triggered by association with **1**, without any terminal phosphido intermediate); the substitution of labile MeCN in another $[\text{LFe}(\text{PCO})(\text{NCMe})]^+$ by the released CO appears to stabilize the *trans*-PCO⁻ ligand in **2**. A ^{31}P NMR recorded after completion of the reaction confirmed that **2** and **3** are formed in equal amounts (Figure S20).

UV-vis monitoring of the reaction of **1** and $\text{Na}(\text{OCP})$ in DMF-d_7 showed the disappearance of the band at $\lambda_{\text{max}} = 444 \text{ nm}$ characteristic for **1** and the appearance of two intense low-energy absorptions at 797 nm ($\epsilon = 1.625 \times 10^4 \text{ L mol}^{-1} \text{ cm}^{-1}$) and 648 nm ($\epsilon = 0.767 \times 10^4 \text{ L mol}^{-1} \text{ cm}^{-1}$) (Figure S38); TD-DFT calculations allowed to assign these prominent bands to electronic transitions within the Fe-P-Fe core of **3** (see below).

Redox properties of **3** in MeCN solution were studied by cyclic voltammetry (CV) and square wave voltammetry (SWV), which revealed two reversible reduction processes at $E_{1/2} = -1.95$ and -2.26 V (vs Fc/Fc^+) as well as an oxidation at $E_{1/2} = -0.6 \text{ V}$ that appears reversible at rt and common scan rates (Figure 4). The first reduction and the oxidation of **3** are significantly shifted to lower potentials compared to the corresponding redox processes of the μ -oxodiferric complex $[(\text{LFe})_2(\mu\text{-O})](\text{OTf})_4$, which shows reduction waves at -1.33 and -2.03 V and a first oxidation at $+0.87$

COMMUNICATION

V. UV-vis spectroelectrochemical monitoring of the oxidation of complex **3** at an applied potential of -0.1 V (vs Fc/Fc⁺) evidenced the disappearance of the signatures of **3** at 797 and 648 nm and the concomitant appearance of a new band at 411 nm with two isosbestic points at 393 and 582 nm. However, prolonged electrolysis at the same potential (-0.1 V) revealed further changes reflected by new isosbestic points at 405 and 566 nm and a shift of λ_{max} from 411 to 423 nm (Figure 5). Subsequent reduction at -1.0 V confirmed chemical reversibility of the two processes and regenerated the original spectrum of **3** (Figure S52). This suggested that **3** can be oxidized twice to sequentially give new complexes **4** ($\lambda_{\text{max}} = 411$ nm) and **5** ($\lambda_{\text{max}} = 423$ nm). Bulk electrolysis of complex **3** at -0.1 V (vs Fc/Fc⁺, Figure S53) indeed indicated that two electrons are transferred at that potential (1.01 mmol, charge passed 0.196 C). To obtain further insight, CV and SWV measurements of **3** as well as **4** and **5** (which both could be isolated; see below) were performed at rt and -35 °C, and at variable CV scan rates (Figures S54 – S56). Criteria such as the increasing separation of the current peaks for the forward and reverse scans (i_{pf} , i_{pr}) at lower temperatures (Figure S54, S55), the decrease of the function $i_{\text{pf}}/v^{1/2}$ with increasing scan rate v (Figure 4), as well as the appearance of a two-humped peak in the SWV of twice oxidized **5** recorded at -35 °C suggest that two electrochemical processes are occurring around -0.6 V and are associated with chemical reactions, the second oxidation of **3** likely being kinetically hindered.

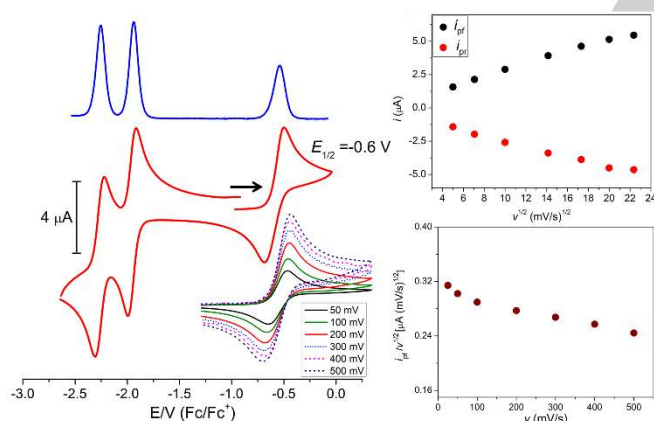


Figure 4. Left: CV (red) and SWV (blue) of **3** in MeCN/0.1 M [nBu₄N]PF₆ at 200 mV/s scan rate; the inset shows the CV of the process at -0.6 V at different scan rates. Right: plots of i_{pf} and i_{pr} versus $v^{1/2}$ (top) and $i_{\text{pf}}/v^{1/2}$ versus scan rate v (bottom) for the process around -0.6 V.

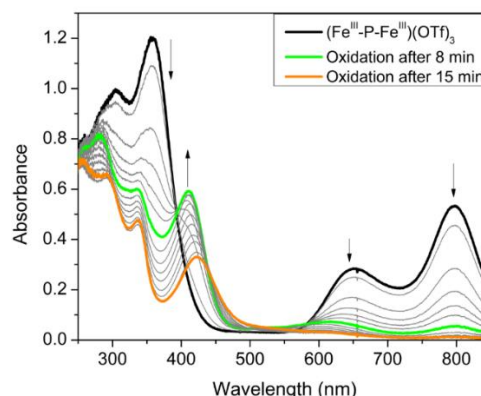


Figure 5. UV-vis spectroelectrochemistry monitoring the first and second oxidation of **3** in MeCN/0.1 M [nBu₄N]PF₆ at an applied potential of -0.1 V (vs Fc/Fc⁺).

UV-vis monitoring during chemical redox titration of a green solution of **3** in MeCN with AgOTf ($E^0(\text{Ag}^+/\text{Ag}) = 0.04$ V vs. Fc/Fc⁺)^[20] showed the same spectral changes: addition of 1 eq. of AgOTf gives a pale green solution of **4** ($\lambda_{\text{max}} = 411$ nm; $\epsilon = 1.35 \times 10^4$ mol⁻¹·cm⁻¹) and addition of further 1.5 eq. of AgOTf leads to further oxidation to give **5** ($\lambda_{\text{max}} = 423$ nm; $\epsilon = 1.05 \times 10^4$ mol⁻¹·cm⁻¹). However, while the first step is fast (within 5 min at rt and 15 min at -35 °C), the second step is kinetically hindered and is completed only after 12 hrs at -35 °C; the final product **5** appears to be unstable and gradually degrades at -10 °C to yield an unknown species with $\lambda_{\text{max}} = 341$ nm (Figure S42).

Bulk oxidation of **3** in MeCN with 1.0 or 2.5 eq. of AgOTf and subsequent precipitation with Et₂O allowed to isolate both the singly and doubly oxidized complexes [(LFe)₂P(MeCN)](OTf)₄ (**4**) and [(LFe)₂P(MeCN)₂](OTf)₅ (**5**), respectively; in the latter case the temperature was kept at -35 °C throughout. Single crystalline material of both new compounds was obtained via slow Et₂O diffusion into MeCN solutions of the crude material. Molecular structures of the cations [(LFe)₂P(MeCN)]⁴⁺ and [(LFe)₂P(MeCN)₂]⁵⁺ are included in Figure 3. Unfortunately, the quality of the crystallographic analysis was poor in the case of **4**; while the overall structure was clearly established, this prevents any discussion of metric parameters. The core structure with an essentially linear Fe-P-Fe dumbbell is preserved throughout the series, but oxidation goes along with an increase in coordination number of the iron ions because of the binding of MeCN ligands *trans* to the μ -P. Hence, mixed-valent **4** features one 5- and 6-coordinate metal ion while both metal ions are 6-coordinate in **5**. This leads to a slight elongation of Fe-P and Fe-C^{NHC} bonds in oxidized **5** compared to parent **3** (Table 1). It can be concluded that MeCN coordination/dissociation is the chemical process associated with the redox couples, leading to electrochemical irreversibility in CVs recorded at low temperatures.

Table 1. Selected bond lengths and angles for complexes **3** and **5**.

	3 (Å)/ degree	5 (Å)/ degree
Fe1-C	1.953(8) - 2.021(7)	1.994(3) - 2.046(2)
Fe2-C	1.951(7) - 2.008(7)	1.993(3) - 2.040(3)
Fe1-P	1.993(2)	2.0079(7)
Fe2-P	1.998(2)	2.0016(7)
Fe1-N	-	1.995(2)
Fe2-N	-	2.013(2)
Fe1-P-Fe2	178.25(12)	179.61(4)

COMMUNICATION

Mössbauer spectra of solid samples of **4** and **5** are included in Figure 3. As expected, the twice oxidized species **5** shows a single quadrupole doublet ($\delta = 0.00$, $\Delta E_Q = 2.69$ mm·s⁻¹) whereas non-symmetric mixed-valent **4** gives rise to two quadrupole doublets of equal intensity ($\delta = 0.02$, $\Delta E_Q = 1.96$ mm·s⁻¹ and $\delta = 0.01$, $\Delta E_Q = 2.68$ mm·s⁻¹). Comparison with the spectra of **3** and **5** allows to assign the former doublet with a smaller quadrupole splitting to the 5-coordinate iron and the latter doublet with a larger quadrupole splitting to the six-coordinate iron in **4**. Interestingly, the IS is essentially invariant for the entire redox series (Table 2). While a cursory interpretation may suggest that oxidation of **3** is purely ligand centered, it should be noted that the IS, which is predominantly a function of the 4s electron contribution to the electron density at the iron nucleus, is influenced by several factors that include the 4s population, the shielding effect due to 3d population, and, more importantly, the Fe–ligand bond lengths that affect the radial extension of the 4s wave function.^[21] Hence the commonly observed negative correlation of IS and oxidation state of the iron center (*viz.*, more negative IS for higher oxidation states) is not strictly valid and may even be reversed in certain cases.^[21] For a series of {FeNO}^x complexes based on tetracarbene macrocycle L, it has been established that the Mössbauer IS cannot be used for a reliable assignment of oxidation states.^[13d] Specifically, the longer Fe-C^{NHC} and Fe-P bonds in oxidized **5** lead to reduced σ -interactions and therefore a less compressed 4s orbital and lower 4s electron density at the iron nucleus, which may counterbalance the effect resulting from depopulating the d orbitals (and decreasing the 4s shielding) upon oxidation.

Table 2. Experimental and DFT calculated (in brackets) ⁵⁷Fe Mössbauer parameters for **3**, **4** and **5**.

	3	4	5
δ [mm s ⁻¹]	0.01 (0.10/0.11)	0.02/0.01 (0.09/-0.04)	0.00 (-0.07/-0.07)
ΔE_Q [mm s ⁻¹]	1.94 (1.74/1.68)	1.96/2.68 (1.72/2.12)	2.69 (2.53/2.52)

SQUID magnetometry of solid samples of **4** and **5** revealed that singly oxidized **4** is an $S = 1/2$ system ($\chi_M T = 0.31$ cm³mol⁻¹K or $\mu_{\text{eff}} = 1.57 \mu_B$ at 295 K; Figure S49), whereas twice oxidized **5** has a well separated $S = 0$ ground state and is diamagnetic over the entire temperature range (2 - 250 K; Figure S50) just as the parent complex **3**. The EPR spectrum of a frozen solution of **4** in MeCN at 163 K (Figure 6) shows an axial spectrum with $g_{x,y} = 2.1059$ and $g_z = 2.0022$ (i.e., $g_z \sim 2$ and $g_{x,y} > 2$) and pronounced hyperfine coupling with the ³¹P nucleus [$A(^{31}\text{P}) = 268.48$ MHz, 271.61 MHz], indicating d_{z²} character of the singly occupied molecular orbital (SOMO) with some P contribution.

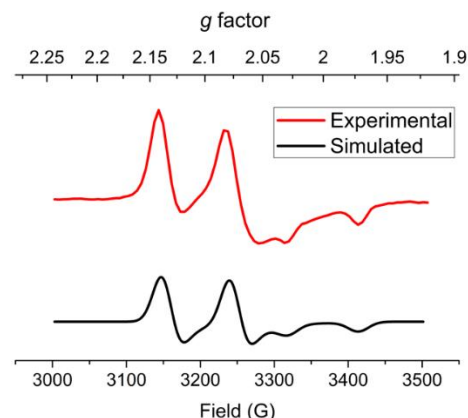


Figure 6. Experimental (top) and simulated (bottom) EPR spectrum of **4** in frozen MeCN (163 K).

The ¹H NMR spectrum of diamagnetic **5** in MeCN-d₃ at 238 K shows only a single set of resonances, indicating that only a single isomer exists or that interconversion of isomers is fast and more facile than in **3** (Figure S30-S35). The ³¹P NMR spectrum of **5** shows a slightly broadened signal at +1122 ppm, low frequency shifted compared to **3** (Figure S36). The ¹H NMR spectrum of **4** is paramagnetic in line with the SQUID and EPR data (Figure S50, S51).

To rationalize the observed spectroscopic signatures and trends, electronic structures of complexes **3** – **5** were examined computationally (see the Supporting Information for details). The DFT results successfully reproduced key geometric parameters and spectroscopic properties within the uncertainty of the computations (Tables S2 and S3), thus lending credence to the proposed electronic structures discussed below.

As shown in Figure 7, the bonding of the (Fe-P-Fe)³⁺ core in **3** entails two π -bonds involving the Fe-d_{xz} and -d_{yz} and P-p_x and -p_y orbitals, and one σ -bond formed by the Fe-d_{z²} and P-p_z orbitals, similar to that found for linear triatomic molecules such as CO₂. Because the system possesses an effective inversion center, only P-p_z can interact with the antisymmetric combination of the Fe-d_{z²} orbitals. The same holds true for the P-p_x and -p_y orbitals. As such, the symmetric combinations of Fe-d_{z²}, -d_{xz} and -d_{yz} orbital are essentially non-bonding in nature, but the one constructed from the two Fe-d_{z²} orbitals is situated slightly higher in energy due to the very weak interaction with the P-s atomic orbital. In the upper valence region of **3**, in addition to the two Fe-d_{xy} orbitals, all the Fe-P-Fe bonding and non-bonding molecular orbitals (MOs) are doubly occupied. Of note, the interaction within the Fe-P-Fe core has substantial covalent-bond character as evidenced by the contributions of the P atom in the σ - and π -bonding MOs being 38% and 50%, respectively. In this situation, it is difficult to unambiguously assign physical oxidation states to the metal ions, although complex **3** can be formally interpreted as having two antiferromagnetically coupled low-spin ferric centers bridged by a P³⁻ ion. The highly covalent Fe-P-Fe interaction accounts for the exceedingly strong antiferromagnetic coupling determined experimentally.

COMMUNICATION

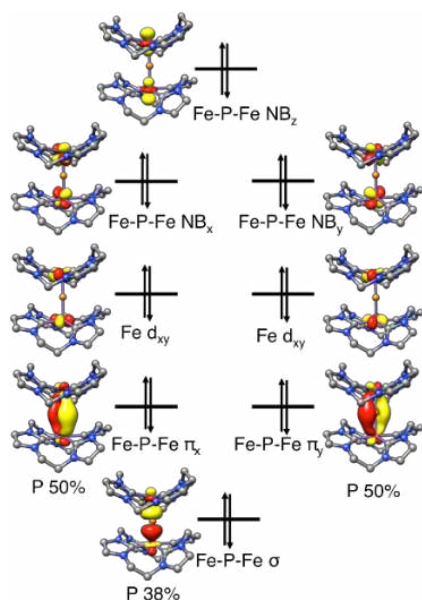


Figure 7. Molecular orbital diagram of complex 3.

Because of lack of inversion symmetry for complex 4, the original Fe-P-Fe nonbonding MOs in 3 acquire some P-p character and polarize toward Fe2 in 4 (Figure 8). Despite of this, comparison of the electronic structures of complexes 3 – 5 (Figures 7, 8 and S63) reveals that upon oxidation the two electrons that reside in the non-bonding MO of 3 with the dominant Fe- d_{z^2} parentage are successively removed. Alternatively, one can rationalize this notion as follows: the energy of this MO should be considerably raised by binding of one or two MeCN molecules to the open axial sites of the Fe ions, because MeCN is a moderate σ -donor and a weak π -acceptor. As a consequence, this MO likely functions as the electron donating orbital upon oxidation. Taken together, the conversion of 3 to 4 and further to 5 is best described as two sequential metal-centered redox processes. The redox active orbital is a non-bonding MO with respect to the Fe-P-Fe interaction; therefore, the Fe-P-Fe core is expected to remain largely intact during oxidation. This is in line with the geometric structures determined experimentally and computationally (Tables 1 and S2). It also accounts for the nearly identical Mößbauer IS measured for complexes 3 – 5, because typically the bond distance between Fe and the strong ligands is a more important factor than the d-electron count for determining the IS shift.^[21,22] The variation of the QS measured for 3 – 5 clearly reflects the variations in coordination number of the Fe sites.

As shown in Figure 8, 4 features a Fe- d_{z^2} centered SOMO that is situated slightly higher in energy than the two fully populated MOs, which possess substantial Fe- d_{xz} and - d_{yz} character and are nearly degenerate. This bonding situation is consistent with its EPR spectrum with $g_z \sim 2$ and $g_{xy} > 2$, similar to a d^9 ion in a trigonal coordination environment with the SOMO being the d_{z^2} orbital.^[23] The SOMO contains marginal contributions from the P-s and - p_z orbitals, in accord with the ^{31}P hyperfine coupling detected by EPR.

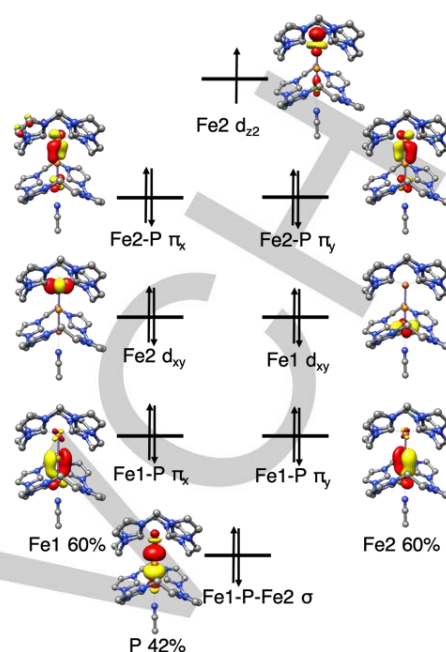


Figure 8. Molecular orbital diagram of complex 4.

TD-DFT calculations suggest that the characteristic low-energy absorption of 3 at 797 nm (Figure S61, Table S3) arises from transitions from the nonbonding Fe- d_{z^2} combination to its σ -antibonding combination, while the band at 648 stems from promoting an α electron from the nonbonding combinations of Fe- d_{xz} and - d_{yz} to the same electron accepting σ^* orbital (see Figure S62). The higher intensity of the former absorption originates from more favorable “overlap” between the electron donating and accepting orbitals.

In summary, a first example of a Fe-(μ -P)-Fe complex with a “naked” bridging phosphido ligand has been isolated, which complements the prominent ferric systems with Fe-(μ -O)-Fe and Fe-(μ -N)-Fe motifs. The macrocyclic tetracarbene scaffold supports the Fe-(μ -P)-Fe core in at least three oxidation states, formally described as ranging from Fe^{III}Fe^{III} to Fe^{IV}Fe^{IV} (reduced congeners of 3 are still being studied). Due to very covalent Fe-P-Fe interaction, however, the physical oxidation state of the metal ions cannot be unambiguously assigned, but the oxidation is clearly metal-based. Complexes with even number of electrons are effectively diamagnetic and the mixed-valent Fe^{III}Fe^{IV} species has a $S = 1/2$ ground state. Sequential twofold oxidation of 3 removes electrons from a nonbonding orbital that originates from the symmetric Fe- d_{z^2} combination, which leaves the structure of the Fe-(μ -P)-Fe core essentially unperturbed. This work underlines the usefulness of the macrocyclic tetracarbene ligand scaffold for isolating unusual Fe (and other 3d metal) complexes, and the potential of Na(OCP) to serve as a P-anion transfer reagent. Future work will address the reductive chemistry of 3, and will focus on elucidating reactivity patterns of the Fe-(μ -P)-Fe motif in its various oxidation states.

COMMUNICATION

Acknowledgements

M.G. is grateful to the Alexander von Humboldt foundation for a postdoctoral fellowship and M.M.H. is grateful to the Fonds of the Chemical Industry for a Liebig scholarship. H.H.C and S.Y. gratefully acknowledge financial support from the Max Planck Society and, in particular, the joint work space of MPI-CEC and MPI-KOFO.

Keywords: iron complexes • phosphido complexes • N-heterocyclic carbenes • redox series • electronic structure

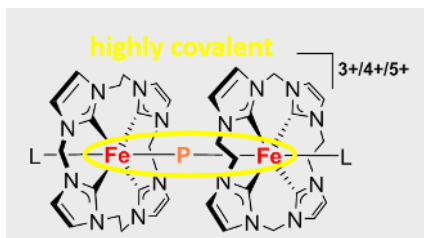
- [1] a) B. M. Cossairt, N. A. Piro, C. C. Cummins, *Chem. Rev.* **2010**, *110*, 4164-4177; b) N. C. Zanetti, R. R. Schrock, W. M. Davis, *Angew. Chem. Int. Ed.* **1995**, *34*, 2044-2046; c) M. Scheer, P. Kramkowski, K. Schuster, *Organometallics*, **1999**, *18*, 2874-2883; d) M. Joost, W. J. Transue, C. C. Cummins; *Chem. Commun.*, **2017**, *53*, 10731-10733. e) P. Kramkowski, G. Baum, U. Radius, M. Kaupp, M. Scheer. *Chem. Eur. J.* **1999**, *5*, 2894-2898. f) M. E. Garcia, V. Riera, M. A. Ruiz, D. Sáez, H. Hamidov, J. C. Jeffery, T. Riis-Johannessen. *J. Am. Chem. Soc.* **2003**, *125*, 13044-13045.
- [2] a) M. Scheer, J. Müller, M. Schiffer, G. Baum, R. Winter. *Chem. Eur. J.* **2000**, *6*, 1252-1257. b) N. C. Mösch-Zanetti, R. R. Schrock, W. M. Davis, K. Wanninger, S. W. Seidel, M. B. O'Donoghue. *J. Am. Chem. Soc.* **1997**, *119*, 11037-11048. c) J. A. Buss, P. H. Oyala, T. Agapie. *Angew. Chem. Int. Ed.* **2017**, *56*, 14502-14506.
- [3] a) E. P. Wildman, G. Balázs, A. J. Wooles, M. Scheer, S. T. Liddle. *Nat. Commun.* **2016**, DOI: 10.1038/ncomms12884. b) C. J. Hoerger, F. W. Heinemann, E. Louyriac, L. Maron, H. Grützmacher, K. Meyer. *Organometallics*, **2017**, *36*, 4351-4354. c) T. M. Rookes, B. M. Gardner, G. Balázs, M. Gregson, F. Tuna, A. J. Wooles, M. Scheer, and S. T. Liddle. *Angew. Chem. Int. Ed.* **2017**, *56*, 10495-10500.
- [4] a) D. M. Kurtz, Jr., *Chem. Rev.* **1990**, *90*, 585-606; b) P. C. Wilkins, H. Dalton, *Biochem. Soc. Trans.* **1994**, *22*, 700-704; c) A. J. Jasniowski, L. Que, *Chem. Rev.* **2018**, *118*, 2554-2592; d) T. Glaser, *Coord. Chem. Rev.* **2019**, *380*, 353-377; e) A. B. Sorokin, *Coord. Chem. Rev.* **2019**, *389*, 141-160.
- [5] a) M. Li, M. Shang, N. Ehlinger, C. E. Schulz, W. R. Scheidt, *Inorg. Chem.* **2000**, *39*, 580-583; b) M. P. Mehn, J. C. Peters, *J. Inorg. Biochem.* **2006**, *100*, 634-643; c) P. Afanasiev, A. B. Sorokin, *Acc. Chem. Res.* **2016**, *49*, 583-593; d) A. B. Sorokin, *Adv. Inorg. Chem.* **2017**, *70*, 107-165.
- [6] a) L. Weber, B. Torwiehe, G. Bassmann, H.G. Stammler, B. Neumann, *Organometallics* **1996**, *15*, 128-132; b) C. Eichhorn, O. J. Scherer, T. Sögdling, G. Wolmershäuser. *Angew. Chem. Int. Ed.* **2001**, *40*, 2859-2861.
- [7] a) O. J. Scherer, T. Hilt, G. Wolmershäuser *Organometallics* **1998**, *17*, 4110; b) M. Scheer, S. Deng, O. J. Scherer, M. Sierka, *Angew. Chem. Int. Ed.* **2005**, *44*, 3755; c) O. J. Scherer, G. Schwarz, G. Wolmershäuser *Z. Anorg. Allg. Chem.* **1996**, *622*, 951; d) S. Yao, T. Szilvási, N. Lindenmaier, Y. Xiong, S. Inoue, M. Adelhardt, J. Sutter, K. Meyer, M. Driess, *Chem. Commun.* **2015**, *51*, 6153; e) F. Spitzer, C. Graßl, G. Balázs, E. M. Zolnhofer, K. Meyer, M. Scheer, *Angew. Chem. Int. Ed.* **2016**, *55*, 4340-4344.
- [8] S. Yao, V. Forstner, P. W. Menezes, C. Panda, S. Mebs, E. M. Zolnhofer, M. E. Miehlich, T. Szilvási, N. A. Kumar, M. Haumann, K. Meyer, H. Grützmacher, M. Driess, *Chem. Sci.* **2018**, *9*, 8590-8597.
- [9] (a) G. Becker, W. Schwarz, N. Seidler, M. Westerhausen *Z. Anorg. Allg. Chem.* **1992**, *612*, 72-82; (b) J. M. Goicoechea, H. Grützmacher, *Angew. Chem. Int. Ed.* **2018**, *57*, 16968-16994.
- [10] (a) F. F. Puschmann, D. Stein, D. Heift, C. Hendriksen, Z. A. Gal, H. F. Grützmacher, H. Grützmacher, *Angew. Chem. Int. Ed.* **2011**, *50*, 8420-8423; b) A. R. Jupp, J. M. Goicoechea, *Angew. Chem. Int. Ed.* **2013**, *52*, 10064-10067.
- [11] see, for example: a) C. Camp, N. Settineri, J. L. Evre, A. R. Jupp, J. M. Goicoechea, L. Maron, J. Arnold *Chem. Sci.*, **2015**, *6*, 6379-6384; b) S. Yao, Y. Xiong, T. Szilvási, H. Grützmacher, M. Driess, *Angew. Chem. Int. Ed.* **2016**, *55*, 4781-4785; c) Y. Xiong, S. Yao, T. Szilvási, E. B. Martínez, H. Grützmacher, M. Driess, *Angew. Chem. Int. Ed.* **2017**, *56*, 4333-4336. d) C. J. Hoerger, F. W. Heinemann, E. Louyriac, L. Maron, H. Grützmacher, K. Meyer, *Organometallics*, **2017**, *36*, 4351-4354; e) L. Weber, *Eur. J. Inorg. Chem.* **2018**, 2175-2227; f) S. Bestgen, Q. Chen, N. H. Rees, J. M. Goicoechea, *Dalton Trans.* **2019**, *47*, 13016-13024.
- [12] S. Meyer, I. Klawitter, S. Demeshko, E. Bill, F. Meyer, *Angew. Chem. Int. Ed.* **2013**, *52*, 901-905.
- [13] a) S. A. Cramer, D. M. Jenkins, *J. Am. Chem. Soc.* **2011**, *133*, 19342-19345; b) M. R. Anneser, S. Haslinger, A. Pöthig, M. Cokoja, J.-M. Basset, F. E. Kühn, *Inorg. Chem.* **2015**, *54*, 3797-3804; c) S. Meyer, O. Krahe, C. Kupper, I. Klawitter, S. Demeshko, E. Bill, F. Neese, F. Meyer, *Inorg. Chem.* **2015**, *54*, 9770-9776; d) C. Kupper, J. A. Rees, S. Dechert, S. DeBeer, F. Meyer, *J. Am. Chem. Soc.* **2016**, *138*, 7888-7898; e) C. Cordes, M. Morganti, I. Klawitter, C. Schremmer, S. Dechert, F. Meyer, *Angew. Chem. Int. Ed.* **2019**, DOI: 10.1002/anie.201900683; f) M. R. Anneser, G. R. Elpitiya, J. Townsend, E. J. Johnson, X. B. Powers, J. F. DeJesus, K. D. Vogiatzis, D. M. Jenkins, *Angew. Chem. Int. Ed.* **2019**, *58*, 8115-8118.
- [14] C. Schremmer, C. Cordes, (née Kupper), I. Klawitter, M. Bergner, C. E. Schiewer, S. Dechert, S. Demeshko, M. John, F. Meyer. *Chem. Eur. J.* **2019**, *25*, 3918-3929.
- [15] S. Ye, C. Kupper, S. Meyer, E. Andris, R. Navrátil, O. Krahe, B. Mondal, M. Atanasov, E. Bill, J. Roithová, F. Meyer, F. Neese, *J. Am. Chem. Soc.* **2016**, *138*, 14312-14325.
- [16] a) J. W. Kück, M. R. Anneser, B. Hofmann, A. Pöthig, M. Cokoja, F. E. Kühn, *ChemSusChem*. **2015**, *8*, 4056-4063; b) M. R. Anneser, S. Haslinger, A. Pöthig, M. Cokoja, V. D'Elia, M. P. Högerl, J.-M. Basset, F. E. Kühn, *Dalton Trans.* **2016**, *45*, 6449-6455; c) C. Kupper, B. Mondal, J. Serrano-Plana, I. Klawitter, F. Neese, M. Costas, S. Ye, F. Meyer, *J. Am. Chem. Soc.* **2017**, *139*, 8939-8949.
- [17] a) L. Liu, D. A. Ruiz, F. Dahcheg, G. Bertrand, R. Suter, A. M. Tondreau, H. Grützmacher. *Chem. Sci.* **2016**, *7*, 2335-2341; b) L. Grant, J. Krzysiek, B. Pinter, J. Telsler, H. Grützmacher, D. J. Mendiola, *Chem. Commun.* **2019**, DOI: 10.1039/c9cc01500k.
- [18] Typically such reactions lead to P-P bond formation, see: a) L. N. Grant, B. Pinter, B. C. Manor, R. Suter, H. Grützmacher, D. J. Mendiola, *Chem. Eur. J.* **2017**, *23*, 6272; b) L. N. Grant, B. Pinter, B. C. Manor, H. Grützmacher, D. J. Mendiola, *Angew. Chem. Int. Ed.* **2018**, *57*, 1049.
- [19] a) M. Scheer, J. Muller, M. Schiffer, G. Baum, R. Winter, *Chem.-Eur. J.* **2000**, *6*, 1252-1257; b) M. C. Fermin, J. Ho, D. W. Stephan, *Organometallics* **1995**, *14*, 4247-4256; c) M. E. Garcia, V. Riera, M. A. Ruiz, D. Saez, H. Hamidov, J. C. Jeffery, T. Riis-Johannessen, *J. Am. Chem. Soc.* **2003**, *125*, 13044-13045.
- [20] a) G. Milazzo, S. Caroli, V. K. Sharma, Tables of Standard Electrode Potentials, Wiley, Chichester, 1978; b) S. G. Bratsch, *J. Phys. Chem. Ref. Data* **1989**, *18*, 1-21.
- [21] Neese, F. *Inorg. Chim. Acta* **2002**, *337*, 181-192.
- [22] a) S. Ye, F. Neese, *J. Am. Chem. Soc.* **2010**, *132*, 3646-3647; b) S. Ye, E. Bill, F. Neese, *Inorg. Chem.* **2016**, *55*, 3468-3474.
- [23] J. A. Weil, J. R. Bolton, *Electron Paramagnetic Resonance: Elementary Theory and Practical Application*, 2nd ed., **2007**, John Wiley & Sons Inc., Hoboken, New Jersey, p 233.

COMMUNICATION

Entry for the Table of Contents

COMMUNICATION

Using a macrocyclic tetracarbene ligand scaffold and Na(OCP) as P-atom transfer reagent allowed to isolate diiron complexes with a "naked" P bridge. The unprecedented linear Fe-(μ -P)-Fe core is highly covalent and is structurally invariant over three oxidation states.



Munmun Ghosh, Hanna H. Cramer, Sebastian Dechert, Serhiy Demeshko, Michael John, Max M. Hansmann, Shengfa Ye,* and Franc Meyer*

Page No. – Page No.

A μ -Phosphido Diiron Dumbbell in Multiple Oxidation States